Electronic Supplementary Material (ESI) for Nanoscale.
This journal is © The Royal Society of Chemistry 2017

Electronic Supplementary Information:

Growth kinetics and mechanisms of multinary copper-based metal sulfide nanocrystals

Keqiang Chen,[1,2,†] Jing Zhou,[1,†] Wen Chen,[1] Qiaohui Zhong,[1] Tingqiang Yang,[1] Xue Yang,[1] Chunyu Deng,[1] Yueli Liu[1,*]

[1] State Key Laboratory of Silicate Materials for Architectures, School of Materials Science and Engineering, Wuhan University of Technology, Wuhan, 430070, P. R. China

[2] College of Electronic Science and Technology, Shenzhen University, Shenzhen, 518060, P. R. China

[*] Correspondent:

Prof. Yueli LIU

Tel.: +86-27-87760159

Fax: +86-27-87760129

E-mail: **lylliuwhut@whut.edu.cn** **(Yueli LIU)**

[†] These authors contribute equally to this study and share first authorship.

Experimental section

Chemicals. Copper(I) iodide (CuI), copper(II) acetate ($Cu(ac)_2$), copper(II) chloride ($CuCl_2$), zinc(II) acetate ($Zn(ac)_2$), zinc chloride ($ZnCl_2$), tin(IV) chloride hydrated ($SnCl_4·5H_2O$), tin(II) chloride ($SnCl_2$), indium(III) chloride ($InCl_3$, 99.9%), antimony(III) chloride ($SbCl_3$, 99%), N,N'-diphenylthiourea (DPT), diphenyl ether, oleylamine (OLA) were purchased from Aladdin Reagent Co. Ltd. Tin (IV) acetate ($Sn(Ac)_4$) was purchased from Alfa Aesar.

Standard synthesis approach for Cu-M-S NCs. A typical hot-injection method was used for the preparation, copper and M precursors were loaded into a 50 mL three-neck flask containing 20 mL OLA. The mixture was heated to a desired temperature under Ar atmosphere, and then a clear slight yellow solution would be emerged. Afterwards, a certain amount of 1M DPT dissolved in diphenyl ether was subsequently injected into the mixture as quickly as possible. The solution was cooled down to room temperature after 5 min. Mother liquor (1 mL) was added into methanol (3 mL) and centrifuged at 8000 rpm for 3 min. Hexane (4 mL) was used to re-disperse the NCs, and the precipitates were separated by the centrifugation at 8000 rpm for 3 min. The product was further purified by several precipitation/dispersion cycles. M represented as Zn, Sn, In and Sb elements. The precursors ratios of Cu:M:S for the preparing of Cu_2ZnSnS_4 (CZTS), Cu_2SnS_3 (CTS), $CuInS_2$ (CIS) and $CuSbS_2$ (CAS) were set as 2:1:1:6, 2:1:4, 1:1:3 and 1:1:3, respectively. The reaction temperatures of CZTS, CTS, CIS and CAS were 190 ℃, 190 ℃, 190 ℃ and 130 ℃, respectively.

The multi-steps reactions. M_1 was loaded into a 50 mL three-neck flask containing 20 mL OLA. The mixture was heated to 190 ℃ under Ar atmosphere to get a clear solution. Afterwards, a certain amount of 1M DPT dissolved in diphenyl ether was subsequently injected into the mixture as quickly as possible, and M_2 dissolved in 2 mL OLA was injected into the above solution after 10 min. Lastly, M_3 (if necessary) dissolved in 2 mL OLA was injected into the above solution after 10 min. The reaction was stopped 10 min after the last metal precursor was injected. The washing process was remained the same with the above strategy. M_n (n = 1-3) represented CuI ($Cu(ac)_2$), $Zn(ac)_2$, $SnCl_4 \cdot 5H_2O$, $InCl_3$ and $SbCl_3$, it was dissolved in oleylamine at 190 ℃ (130 ℃ for $SbCl_3$) under Ar atmosphere to form clear solutions, the metal precursors could present at any step of the reaction randomly.

Synthesis of various binary metal sulfides NCs. In order to remove the other possible influence factors, we prepared the metal sulfides NCs (Cu_2S (CuI as copper precursor), $Cu_{2-x}S$ ($Cu(ac)_2$ as copper precursor), ZnS, SnS_2, In_2S_3 and Sb_2S_3) through the aforementioned standard procedure but only one metal precursor (CuI, $Cu(ac)_2$, $Zn(ac)_2$, $SnCl_4 \cdot 5H_2O$, $InCl_3$ or $SbCl_3$) was used for each NCs synthesis processes of the corresponding metal sulfide. Moreover, the reaction temperatures of $Cu_{2-x}S$, ZnS, SnS_2 and In_2S_3 NCs were set as 190 ℃, and the various reaction times (1 min, 10 min, 3 min and 5 min) were used to get the desired sizes. Moreover, the reaction temperatures of Cu_2S and Sb_2S_3 NCs were set as 130 ℃ with the reaction time of 1 and 10 min, respectively.

Cation exchanging reaction. Various binary metal sulfides were synthesized through the aforementioned '**Synthesis of various binary metal sulfides NCs**' approach, and re-dissolved in OLA after washing out the unreacted precursors. Whereafter, the as-prepared binary metal sulfides NCs were dissolved in 20 mL OLA after the temperature of this solution reached to 190 ℃ (130 ℃ for CAS), and the other metal ions dissolved in 2 mL OLA were injected into the above solution. The solution was cooled to room temperature after 10 min. The washing process was remained the same with the above strategy. The reaction process was under Ar atmosphere.

Inter-reaction between binary metal sulfides. Various binary metal sulfides were synthesized through the aforementioned "**Synthesis of various binary metal sulfides NCs**" approach, and re-dissolved in 2 mL OLA after washing out the unreacted precursors. Different kinds of binary metal sulfides OLA solutions were injected simultaneously into 20 mL pre-heated (190 ℃ for CZTS, CTS and CIS; 130 ℃ for CAS) OLA. The reaction was stopped after 10 min under Ar atmosphere. The washing process was remained the same with the above strategy.

Characterization. The crystal structure and microstructure of the as-prepared NCs were characterized by X-ray diffraction (XRD, Pert-Pro, PANalytical, Netherlands), and transmission electron microscope (TEM, JEM-2100F, JEOL, Japan). Energy dispersive energy dispersive X-ray (EDX) data were collected as an ensemble measurement in a field emission scanning electron microscope (FESEM, JSEM-5610LV). UV-vis absorption spectrum (UV-2550, Shimadzu, Japan) was recorded to characterize the optical absorption properties of the samples. Raman spectroscope (Raman, Renishaw Invia, Britain) equipped with a 633 nm laser was employed to get the structural information. The samples were also analyzed by X-ray photoelectron spectroscopy (XPS, ESCALAB 250Xi, America) with monochrome Al Kα radiation.

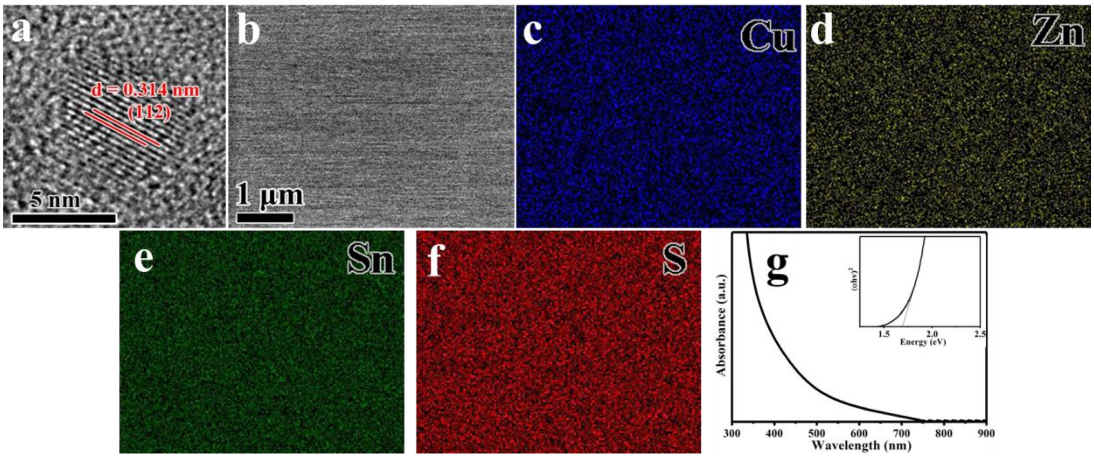

Fig. S1 High resolution TEM image (a), FESEM image (b), corresponding EDX mapping (c)-(f), and UV-vis absorption spectrum (inset shows the corresponding absorption band edge estimated by Tauc plots) (g) of CZTS NCs prepared through the standard approach. The metal precursors are CuI, $Zn(ac)_2$ and $SnCl_4\cdot5H_2O$. These results indicate that the as-prepared product is pure CZTS. From the EDX mapping, one can clear to see that the four elements, including Cu, Zn, Sn, and S, are homogeneously distributed, which indicates that the as-prepared CZTS NCs have a uniform composition without a second phase.

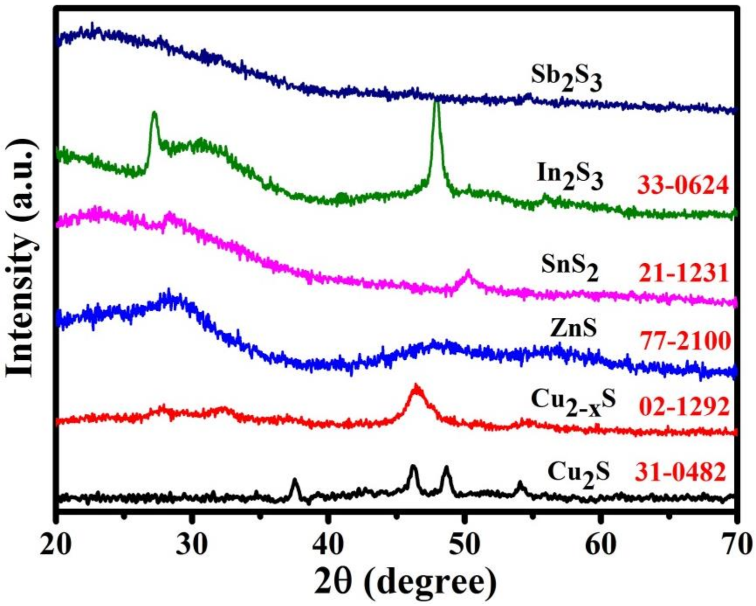

Fig. S2 XRD patterns of various binary metal sulfides prepared through the "Synthesis of various binary metal sulfides NCs" approach. The metal precursors are CuI, Cu(ac)$_2$, Zn(ac)$_2$, SnCl$_4$·5H$_2$O, InCl$_3$ and SbCl$_3$, which correspond to Cu$_2$S, Cu$_{2-x}$S, ZnS, SnS$_2$, In$_2$S$_3$ and Sb$_2$S$_3$, respectively. From their standard PDF cards, we can find that the as-prepared Cu$_2$S, Cu$_{2-x}$S, ZnS, SnS$_2$, In$_2$S$_3$ and Sb$_2$S$_3$ NCs are orthorhombic, cubic, cubic, hexagonal, hexagonal and amorphous structures, respectively.

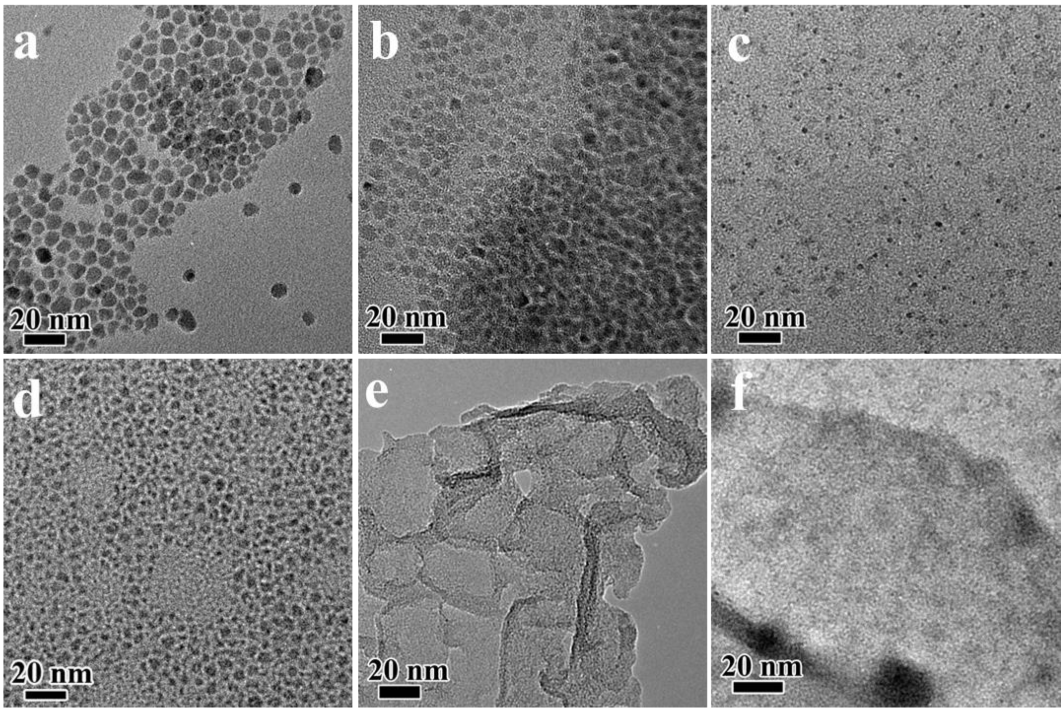

Fig. S3 TEM images of various binary metal sulfides prepared through the ‘Synthesis of various binary metal sulfides NCs’ approach. Panels a-f correspond to Cu_2S, $Cu_{2-x}S$, ZnS, SnS_2, In_2S_3 and Sb_2S_3, respectively. The metal precursors are CuI, $Cu(ac)_2$, $Zn(ac)_2$, $SnCl_4 \cdot 5H_2O$, $InCl_3$ and $SbCl_3$, respectively. The sizes of the NCs are 7.57, 5.34, 2.61 and 4.12 nm corresponding to panels a-d, respectively. While panels e and f show as nanosheets (In_2S_3) and amorphous state (Sb_2S_3), respectively.

Note: The structure of In_2S_3 can be indexed as γ-In_2S_3, hexagonal phase. Moreover, the In_2S_3 nanosheets are formed through top-down processes.[1]

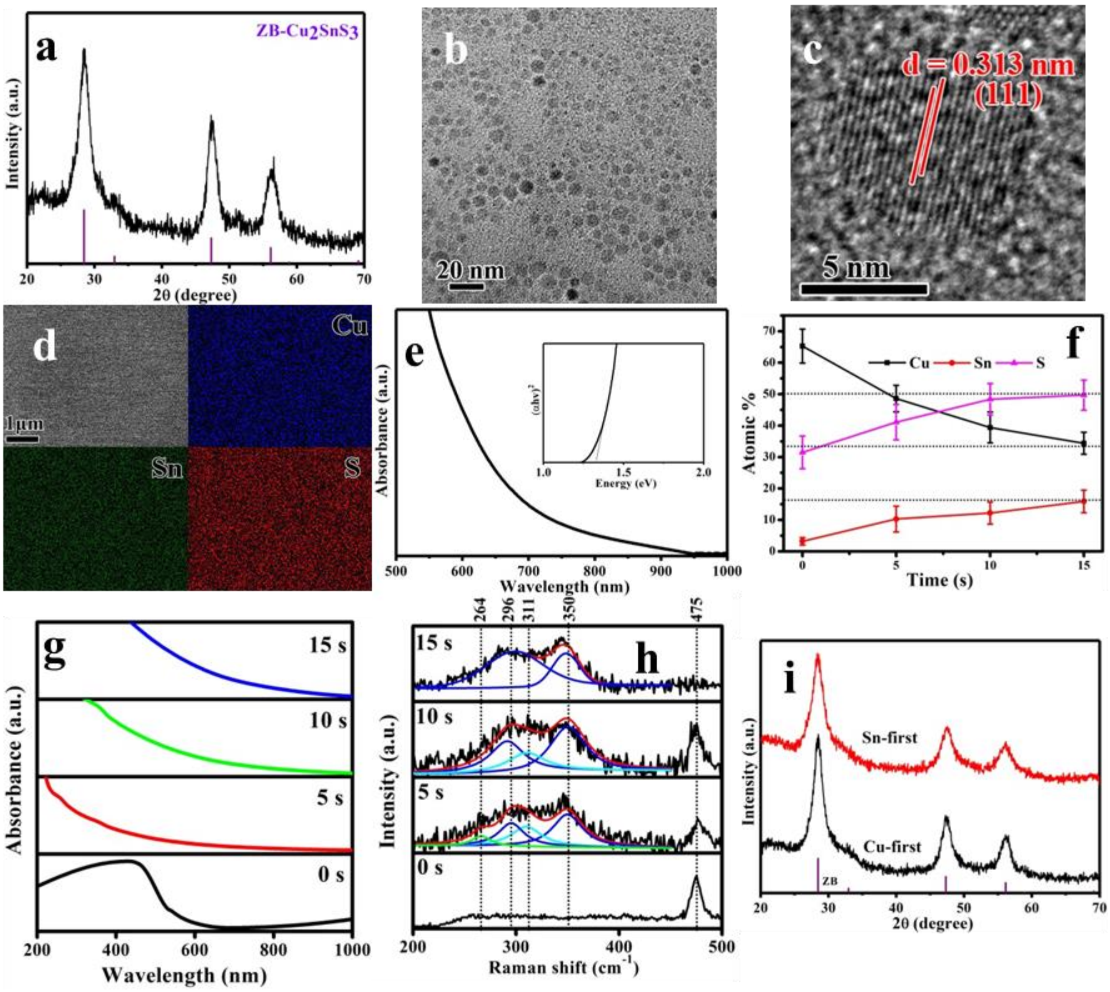

Fig. S4 XRD pattern (a), TEM image (b), high resolution TEM image (c), FESEM image and corresponding EDX mapping (d), UV-vis absorption spectrum (inset shows the corresponding absorption band edge estimated by Tauc plots) (e), reaction time dependent EDX (f), UV-vis absorption (g) and Raman (h) spectra of CTS NCs prepared through the standard approach. (i) XRD pattern of CTS NCs prepared through the multi-steps reactions. The metal precursors are CuI and $SnCl_4 \cdot 5H_2O$. The EDX mapping results suggest Cu, Sn, and S are homogeneously distributed, which indicates the phase purity of as-prepared CTS NCs. The Raman peaks at 264 and 475 cm^{-1} can be indexed as Cu_xS, and the peak at 311 cm^{-1} corresponds to SnS_2, the other peaks (296 and 350 cm^{-1}) are close to the values reported for CTS.

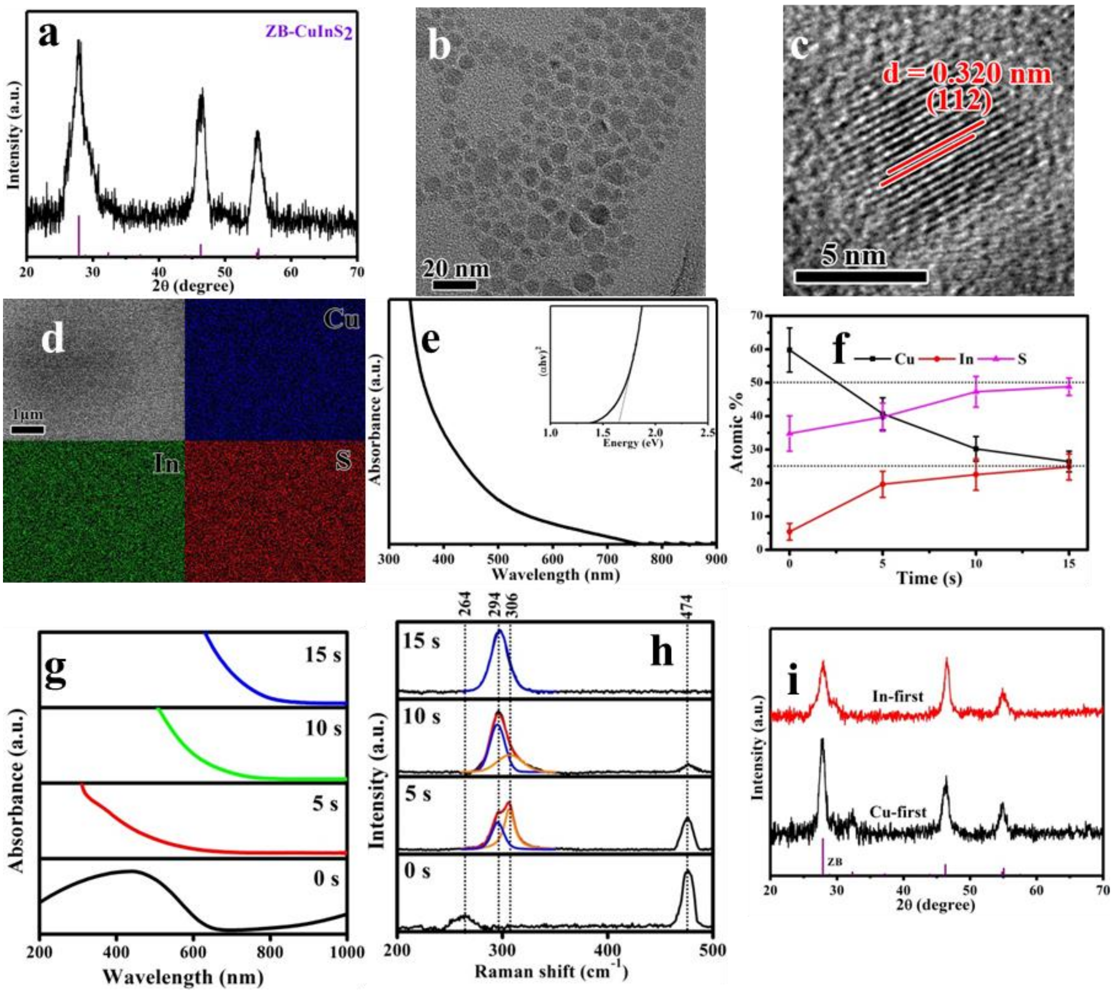

Fig. S5 XRD pattern (a), TEM image (b), high resolution TEM image (c), FESEM image and corresponding EDX mapping (d), UV-vis absorption spectrum (inset shows the corresponding absorption band edge estimated by Tauc plots) (e), reaction time dependent EDX (f), UV-vis absorption (g) and Raman (h) spectra of CIS NCs prepared through the standard approach. (i) XRD pattern of CIS NCs prepared through the multi-steps reactions. The metal precursors are CuI and $InCl_3$. From panel d, it’s easy to find that the three elements, including Cu, In, and S, are homogeneously distributed, which indicates that the as-prepared CIS NCs have a uniform composition without a second phase. The Raman peaks at 264 and 474 cm^{-1} can be indexed as Cu_xS, and the peaks at 306 and 294 correspond to In_2S_3 and CIS, respectively.

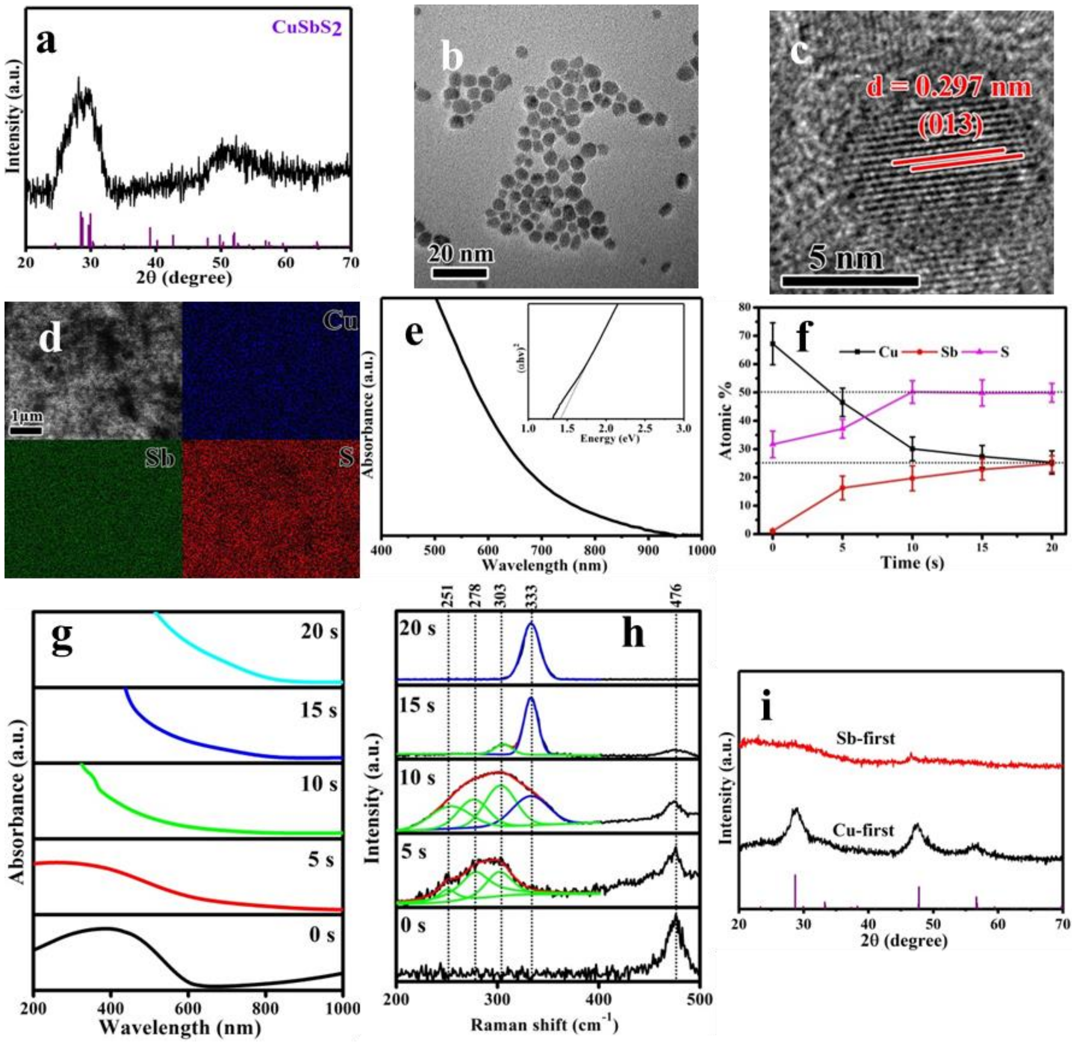

Fig. S6 XRD pattern (a), TEM image (b), high resolution TEM image (c), FESEM image and corresponding EDX mapping (d), UV-vis absorption spectrum (inset shows the corresponding absorption band edge estimated by Tauc plots) (e), and reaction time dependent EDX (f), UV-vis absorption (g), and Raman (h) spectra of CAS NCs prepared through the standard approach. (i) XRD pattern of CAS NCs prepared through the multi-steps reactions. The metal precursors are CuI and $SbCl_3$. The EDX mapping results suggest Cu, Sb, and S are homogeneously distributed, which indicates the phase purity of as-prepared CAS NCs. The Raman peak at 476 cm^{-1} can be indexed as Cu_xS, and the peaks at 251, 278, and 303 cm^{-1} correspond to Sb_2S_3, the peak at 333 cm^{-1} are close to the values reported for CAS.

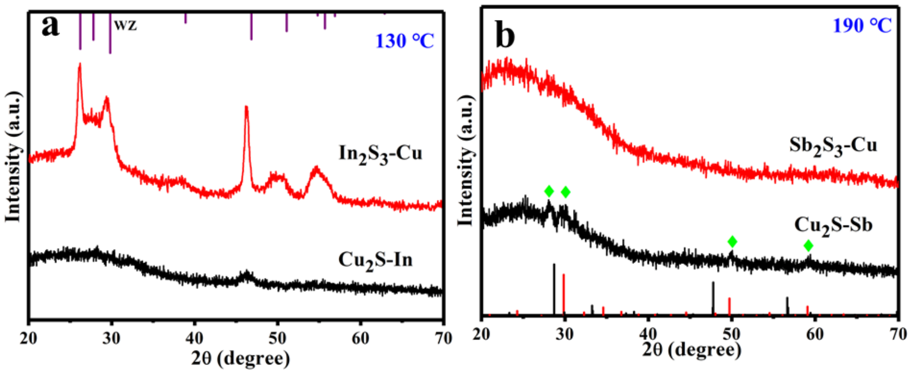

Fig. S7 XRD patterns of the samples prepared through the cation exchanging reactions at various temperatures. The metal precursors are CuI and $InCl_3$ for panel a, CuI and $SbCl_3$ for panel b, respectively.

Discussions on the cation exchanging reactions.

Previous reports indicate that the cation exchanging process would break the initial crystal structure to some extent.[1-3] Moreover, the rates of the incoming and outgoing cations should keep balance to avoid the broken down of the initial crystal structure, that is to say, the crystal structure would be destroyed when the rate of outgoing cation is bigger than that of the incoming cation.[3] It's well known that Cu_2S is in the superionic conducting state at high temperature,[4, 5] which indicates that the copper ions have high mobility.[6-8] In the cation exchanging reactions, it is noteworthy that the reactions of CZTS, CTS and CIS NCs are put into effect at 190 ℃, while the reaction temperature of CAS NCs is set as 130 ℃. Accordingly, CIS and CAS NCs are selected to study the influence of reaction temperatures on the cation exchanging reactions (Fig. S6). For Cu_2S based cation exchanging reactions, comparing Fig. S6a with Fig. 3c, one can clearly see that even though no expected crystal structures have been achieved for the reactions of CIS NCs at low temperature (130 ℃), the final samples present as a poor crystallized Cu_2S phase. Moreover, for the reaction of CAS NCs at 190 ℃, the product is shown as a mixture of Cu_3SbS_4 and $Cu_{12}Sb_4S_{13}$ phases, while the crystallinity reduces sharply. These results suggest that the reaction temperature is an important factor for the cation exchanging reactions, which would change the mobility of copper ions. However, even though the reaction temperatures have effects on the crystallinity of as-prepared samples, the crystal structures have not been modified. In addition, the M_yS (M = In and Sb) based cation exchanging reactions have rare relationships with the reaction temperature (Fig. S6). Accordingly, there should have some other crucial issues.

The cation exchanging process is replacing the origin cation with a new one, and if the difference between these two ionic radii is relatively large, a great lattice distortion might emerge. That is to say, the big radius variety between Cu (77 pm) and Sn (69 pm) [9] would lead to the ruination of the origin crystal structure, regardless of the basic crystal structure, reaction temperature and the mobility of cation ions. We believe that this might be the reason for the amorphization of cation exchanging reactions of CZTS and CTS samples. On the contrary, the nearly same radii of Cu and Sb (76 pm) [10] could result in the maintenance of the initial crystal structures as the regular one as possible. As the Sb_2S_3 used in the cation exchanging reactions is amorphous state, no Cu-Sb-S phase could be obtained. For Cu-In-S system, the high mobility of copper ions, as well as the relatively bigger ionic radius of In (80 pm) [11] would lead to the fact that the outgoing rate of copper ions (Cu_{out}) is much larger than the incoming rate of indium ions (In_{in}) if the growth process is based on the Cu_2S structure at various temperatures, which would destroy the crystal structure of Cu_2S phase. While, if the cation exchanging reaction is based on the In_2S_3 structure, the low mobility of indium ions could keep the balance of the incoming and outgoing rates of the ions. Moreover, the medium discrepancy of Cu and In ionic radii is another important factor for maintaining the stabilization of the origin In_2S_3 structure during the cation exchanging process, as a result, $CuInS_2$ NCs could be obtained.

Discussions on the phase transformations of copper antimony sulfide NCs during the cation exchanging reaction and inter-reaction between binary metal sulfides processes.

Copper antimony sulfide is a p-type material with four major phases, namely, $CuSbS_2$, Cu_3SbS_3, $Cu_{12}Sb_4S_{13}$ and Cu_3SbS_4.[12] The varieties of the compositions of copper antimony sulfide could lead to different phases, and the phase tunability of copper antimony sulfide NCs can be achieved by adjusting the ratio of various precursors.[13] Previous works suggested that prolonging the reaction time or increasing the reaction temperature could lead to the enhancement of the content of Sb in the final product, which results in the phase transformation from $Cu_{12}Sb_4S_{13}$ to $CuSbS_2$.[14] During the cation exchanging reaction and inter-reaction between binary metal sulfides processes, we assume that the relative big size of Cu_xS original structure is disadvantageous to the addition of Sb, which leads to the formation of Cu_3SbS_4 phase.

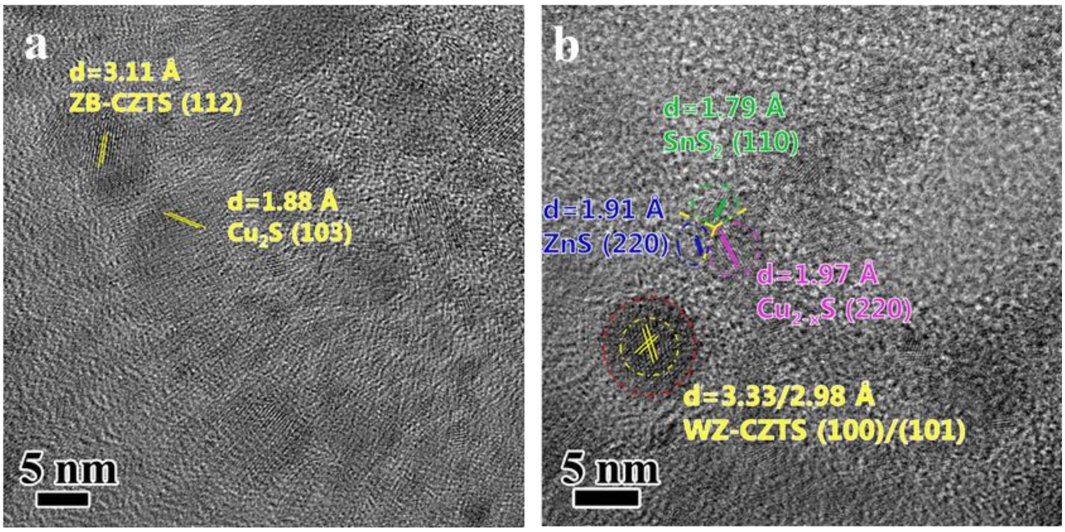

Fig. S8 TEM images of the products prepared through the inter-reaction between binary metal sulfides for 1 min. The binary metal sulfide NCs are Cu_2S (7.57 nm), ZnS(2.61 nm) and SnS_2 (4.12 nm) for panel a, and $Cu_{2-x}S$ (5.34 nm), ZnS(2.61 nm) and SnS_2 (4.12 nm) for panel b.

Discussions on the phase transformations of CZTS NCs during the inter-reaction between binary metal sulfides.

The inter-reactions between binary metal sulfides (Cu_xS, ZnS and SnS_2) for the preparation of CZTS have been investigated for further investigating the reaction kinetics. Fig. S7a shows the TEM image of product prepared through the inter-reaction between binary metal sulfides (Cu_2S, ZnS and SnS_2, corresponding to Fig. 4) for 1 min. It's clear to see that several bigger size NCs (ZB structure CZTS or Cu_2S) and huge amounts of smaller size NCs (might be ZnS and SnS_2) co-exist in the product, and the smaller ones surround the bigger ones. It indicates that the bigger Cu_2S NCs are in relatively homogeneous surroundings (smaller NCs), which might promote the growth of different crystal planes with similar growth rates, and the formation of CZTS during this reaction might undergo an isotropic growth. Furthermore, TEM image of the product prepared through the inter-reaction between $Cu_{2-x}S$, ZnS and SnS_2 for 1 min is shown in Fig. S7b (corresponding to Fig. 7a), it's clear to see that many boundaries of different NCs have arisen, which indicates the inter-reaction of binary metal sulfide NCs is ongoing. A representative combination has been studied in detail, three phases including $Cu_{2-x}S$ (pink), ZnS (blue) and SnS_2 (green) could be observed, which reveals that the reaction is in progress under an asymmetric contact, which might lead to the different growth rates for various crystal planes. In comparation with these TEM images, it's easy to find that the larger or smaller size differences of binary metal sulfide NCs lead to different ways through which the NCs contact, as well as different reaction surroundings. As a result, the growth pathways of these two reactions have great differences with each other (isotropic or anisotropic growth), and CZTS NCs with ZB or WZ structures emerge.

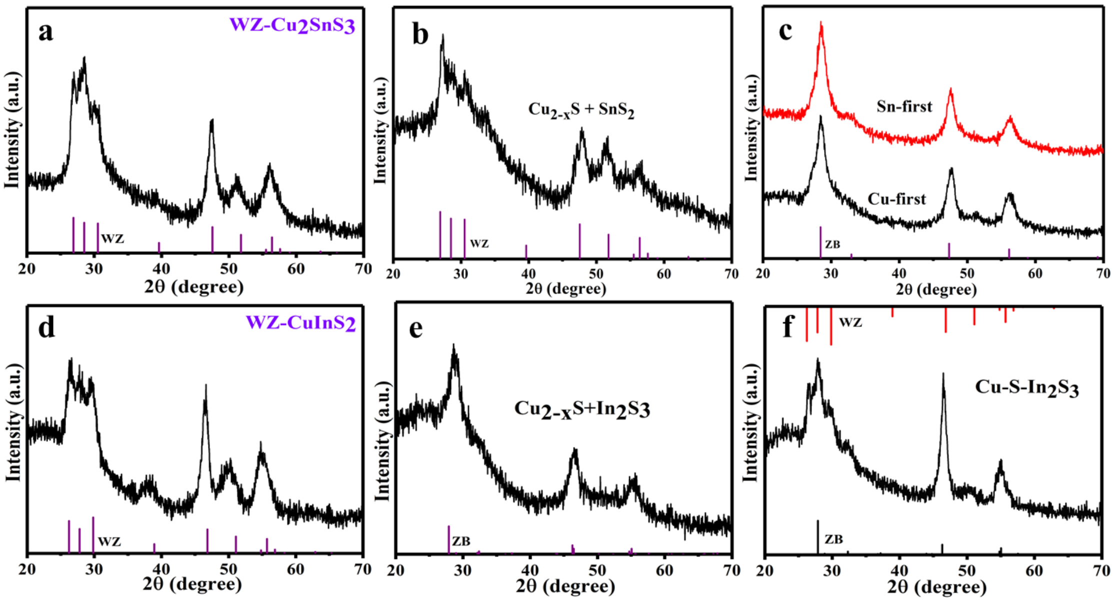

Fig. S9 XRD patterns of the products prepared through the standard approach (a) and (d), inter-reaction between binary metal sulfides (b) and (e) and multi-steps reactions (c). (f) XRD pattern of CIS NCs prepared through the multi-steps reaction by replacing indium precursor with In_2S_3 nanosheets. The copper precursor is $Cu(ac)_2$ for all the reactions. $SnCl_4 \cdot 5H_2O$ is used as tin precursor for the reactions in panels a-c, $InCl_3$ is used as indium precursor for the reactions in panels d-f.

Notes and references

1. S. Sarkar, A. D. P. Leach and J. E. Macdonald, *Chem. Mater.*, 2016, **28**, 4324-4330.

2. D. H. Son, S. M. Hughes, Y. Yin and A. Paul Alivisatos, *Science*, 2004, **306**, 1009-1012.

3. W. van der Stam, A. C. Berends, F. T. Rabouw, T. Willhammar, X. Ke, J. D. Meeldijk, S. Bals and C. de Mello Donega, *Chem. Mater.*, 2015, **27**, 621-628.

4. S. T. Connor, C.-M. Hsu, B. D. Weil, S. Aloni and Y. Cui, *J. Am. Chem. Soc.*, 2009, **131**, 4962-4966.

5. K. Wakamura and I. Tsubota, *Solid State Ionics*, 2000, **130**, 305-312.

6. S. Cassaignon, T. Pauporté, J.-F. Guillemoles and J. Vedel, *Ionics*, 1998, **4**, 364-371.

7. K. Wakamura, *Phys. Rev. B*, 1997, **56**, 11593-11599.

8. Q. Li, L. Zhai, C. Zou, X. Huang, L. Zhang, Y. Yang, X. Chen and S. Huang, *Nanoscale*, 2013, **5**, 1638-1648.

9. M. Li, W.-H. Zhou, J. Guo, Y.-L. Zhou, Z.-L. Hou, J. Jiao, Z.-J. Zhou, Z.-L. Du and S.-X. Wu, *J.Phys. Chem. C*, 2012, **116**, 26507-26516.

10. R. Asai, H. Nemoto, Q. Jia, K. Saito, A. Iwase and A. Kudo, *Chem. Commun.*, 2014, **50**, 2543-2546.

11. J.-H. Lee and B.-O. Park, *Thin Solid Films*, 2003, **426**, 94-99.

12. K. Ramasamy, H. Sims, W. H. Butler and A. Gupta, *Chem. Mater.*, 2014, **26**, 2891-2899.

13. K. Chen, J. Zhou, W. Chen, Q. Chen, P. Zhou and Y. Liu, *Nanoscale*, 2016, **8**, 5146-5152.

14. Y. Zou and J. Jiang, *Mater. Lett.*, 2014, **123**, 66-69.